Adaptive Iso-Altitude Tracking and Terrain Reconstruction by Submarine Vehicle Formations

Shahab Kalantar, Uwe Zimmer

Australian National University
Department of Information Engineering
Canberra, ACT 0200, Australia
shahab.kalantar@rsise.anu.edu.au,uwe.zimmer@ieee.org

Abstract

In this paper, we address the problem of partial reconstruction of underwater landscape in a region using a group of formations of autonomous cooperating vehicles. Sampling is adaptive in that only a small set of iso-contours are sampled, as opposed to the more traditional strategy of sampling along pre-defined trajectories sweeping unnecessary areas. To achieve this, we model the environment as a tesselation of the plane by triangular elements with linear interpolation inside each element. Each formation consists of three cooperating vehicles which traverse the tesselation element-wise by computing ascent (descent) directions using the simplex algorithm and climbing to reach a specific isocline. We extend the standard simplex algorithm to the case of moving over iso-contours.

1 Introduction

A major application of underwater robots is to survey a particular phenomenon and gain knowledge about its structure. We can conveniently think of these phenomena (called fields , henceforth) as functions defined on the plane. One naive strategy is to have a collection of vehicles cover the whole region in which the field is defined (for example, by following parallel transects along the length of the field). This would require resolving issues of localization with respect to an external beacon and, moreover, a lot of space should be sampled unnecessarily. Desirable would be a strategy which uses the field itself for localization and only samples those areas which are structurally important (such as those with high gradients).

To motivate, consider this specific scenario: an initial aggregate of autonomous underwater vehicles (such as *Serafina* [Serafina web site], figure 1(a)), residing on a plane parallel to the surface of the ocean, self-organizes itself into a set of small formations with identical numbers of robots which are then dispatched to reach different specific iso-contours of the underwater landscape beneath, adaptively sample them, rendezvous back to the initial place, and merge into one coherent group. The samples can then be used to reconstruct the terrain using interpolation [Horman et al., 2003]. The fidelity of the reconstruction is a function of the particular iso-contours sampled and the quality of approximation of each iso-contour. Achieving this goal implies, among others, that individual formations be capable of computing reliable descent directions and advancing along them (or perpendicular to them for iso-contour traversal). This capability clearly shows the relation between this application and optimization theory, where the goal is to localize optima. Terrain reconstruction is only considered here as an example. The described technique can be used for identifying any field (such as salinity).

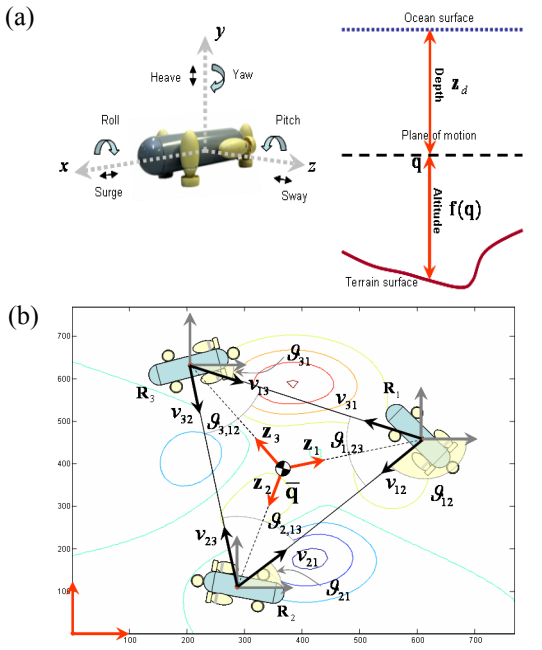

figure 1: (a) Terrain observation. (b) Simplex formation.

For a smooth terrain, the steepest descent direction (gradient and conjugate gradient) can be used. The iterative solution (with a specified initial value) follows a continuous trajectory towards a local optimum.

For vehicles equipped with only altitude-measuring sensors, though, the gradient has to be estimated (e.g., using finite differences), justifying the need for deploying multiple platforms. Such an approach models the environment by its first or second order approximation around a local optimum. Gradient and Hessian are unknown parameters of this model.

[Rendas et al., 2002], [Reet, 2005], [Zhang and Leonard, 2005], [Ogren et al., 2002], [Robinet, 2004], [Pang et al., 2003], [Burian et al., 1996] are a sample of papers where this strategy has been employed.

For non-smooth noisy objective functions, *zero-order* methods have been devised which can be roughly classified into *derivative-free* and *direct search* methods. In these methods, the solution jumps from one iterate to the other. Of particular interest to us is the direct search method known as the *basic simplex* method [Kolda et al., 2003]. In this method, a nondegenerate triangle, initialized somewhere on the plane, plays the role of the initial solution. At each iterate, the worst vertex (one with the lowest or the highest value, depending on case) is reflected around the opposite edge, producing a new triangle (solution). This corresponds to moving from one element to an adjacent one in a tesselation of the plane (defined by the size and orientation of the initial element). The main reason behind *robustness* of such methods is that, at each iterate, a small number of actions (3 for the simplex method) are available. *Deciding on which of the three actions (reflections) to take only depends on relative sensor measurements and not on the exact values.* This leaves for large noises without affecting the trajectory. See [Kolda et al., 2003] for a review of direct-search methods and [Burian et al., 1996], [de Sousa et al., 2005], [Speranzon et al., 2004] for previous research where the simplex method has been used solely for locating optima. In our previous paper [Kalantar and Zimmer, 2007], linear interpolation was used to model the terrain inside each element. This model was then used to define a strategy for reflecting over an isocline. In this paper, we use rotation of the formation to implement reflection and add an additional adjustment phase to reduce uncertainty when reflecting over isoclines. For clarity's sake, we will only consider the case where the environment is smooth and there is no sensor or actuator noise. A short discussion of these issues appears in section 6.

1.1 Simplex Formations

In this paper, we consider planar regular triangular formations $\boldsymbol{S}\{\mathbf{q}_1, \mathbf{q}_2, \mathbf{q}_3\}$ ($\boldsymbol{S}$ for short) of underwater vehicles $\boldsymbol{R}_1$, $\boldsymbol{R}_2$ and $\boldsymbol{R}_3$, residing on a horizontal plane $\mathbf{P}$ parallel to the surface of the ocean characterized by a given *depth* z_d, with positions (vertices) $\mathbf{q}_1$, $\mathbf{q}_2$ and $\mathbf{q}_3$, $\mathbf{q}_i = (x_i, y_i)^T \in \Re^2$, measured with respect to some inertial reference system $\Upsilon_{\mathbf{P}}$ attached to $\mathbf{P}$. Define $\mathbf{q}_{\boldsymbol{S}} = (\mathbf{q}_1, \mathbf{q}_2, \mathbf{q}_3)^T$. Denote by $\boldsymbol{e}_{ij} = \boldsymbol{e}_{ji}$ the edge between $\boldsymbol{R}_i$ and $\boldsymbol{R}_j$, and by $\boldsymbol{v}_{ij} = \mathbf{n}(\mathbf{q}_j - \mathbf{q}_i) = -\boldsymbol{v}_{ji}$ the edge vector, where $\mathbf{n}(\mathbf{u}) = \mathbf{u}/\|\mathbf{u}\|$. We also use $\boldsymbol{S}$ to denote the inside and edges of the triangle. Any point $\mathbf{p}_w \in \boldsymbol{S}$ can be expressed as the linear combination $\mathbf{p}_w = \boldsymbol{w} \cdot \mathbf{q}_{\boldsymbol{S}}$ where $\boldsymbol{w} = (w_1, w_2, w_3)^T$ is the *barycentric* coordinates of $\mathbf{p}_w$. Thus, the centre of mass $\bar{\mathbf{q}}_{\boldsymbol{S}}$ is given by $(1/3, 1/3, 1/3)$. For any $\mathbf{p}_w \in \boldsymbol{S}$, define $\mathbf{z}_{\mathbf{p}_w, i} = \mathbf{n}(\mathbf{q}_i - \mathbf{p}_w)$. Also denote $z_i \equiv z_{\bar{\mathbf{q}}_{\boldsymbol{S}}, i}$. Denote by $\vartheta_{i,jk}$ the angle between v_{ij} and v_{ik}, and define $L_{ij} = L_{ji} = \|\mathbf{q}_j - \mathbf{q}_i\|$. Associate local coordinate frames Υ_i, aligned with $\Upsilon_{\mathbf{P}}$, with every robot. Denote by ϑ_{ij} the bearing of $\mathbf{q}_j$ with respect to Υ_i. If $\boldsymbol{A}_d$ denotes a desired size for the triangle, the desired side lengths (values for L_{ij}) are given by

$$\boldsymbol{L}_d = \left(\frac{2\boldsymbol{A}_d}{\sin(\pi/3)}\right)^{1/2}. \tag{1}$$

Also, $\vartheta_{3,12} = \vartheta_{1,23} = \vartheta_{2,13} = \pi/3$. We will limit our treatment to the case of *clock-wise* formations. In such a triangle, clock-wise traversal of the edges will visit the vertices in the order $1 \to 2 \to 3$. Figure 1 shows a formation together with the defined terms.

Denoting by $\Omega \subseteq \Re^2$ the closed region of operation, the landscape beneath $\mathbf{P}$ defines a function $\mathbf{f}: \Omega \to \Re$. Robots sample this function by measuring the altitude, providing the vector $\mathbf{f}_{\boldsymbol{S}} = [\mathbf{f}(\mathbf{q}_1), \mathbf{f}(\mathbf{q}_2), \mathbf{f}(\mathbf{q}_3)]^T$.

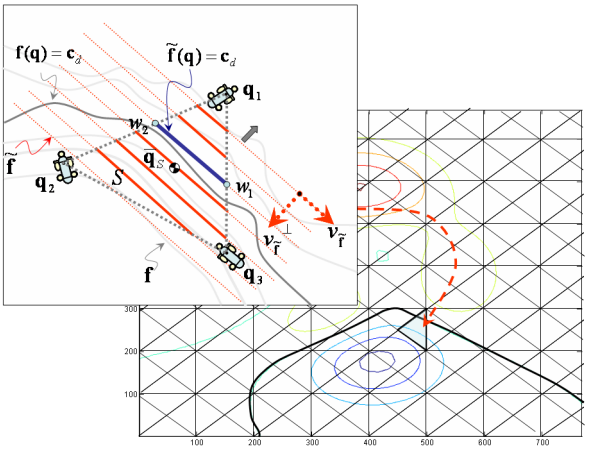

figure 2: Environmental modeling and linear interpolation by triangular elements.

2 Modeling the environment

In this section, we present an approach to modeling the field which is basically the same one used in finite element literature. Refer to figure 2 for illustration.

2.1 Linear Interpolation

Let $\Omega \subseteq \Re^2$ be a (closed) domain on the plane. A *triangulation* $\boldsymbol{T}_h(\Omega) = \{\boldsymbol{S}_\alpha\}$ of Ω is the division of Ω into triangles $\boldsymbol{S}_\alpha$ in such a way that each triangle side is shared *only* by *adjacent* triangles. This means that the triangles can only touch each other but not overlap (*contiguity*). Two triangles $\boldsymbol{S}_\alpha$ and $\boldsymbol{S}_\beta$ are called adjacent if they share a side. A *tesselation* is a regular *tiling* (*plane-filling arrangement*) of regular triangles. We denote by $\boldsymbol{P}_1(\Gamma)$ the space of all linear functions of the form

$$v(\mathbf{q}) = a_{00} + a_{10}x + a_{01}y, \tag{2}$$

where $\mathbf{q} \in \Gamma$, $\mathbf{q} = (x, y)$, and $a_{ij} \in \Re$. The basis functions for $\boldsymbol{P}_1(\Gamma)$ are $\psi_1(\mathbf{q}) = 1$, $\psi_2(\mathbf{q}) = x$ and $\psi_3(\mathbf{q}) = y$.

A *finite element* is a triple $\langle \boldsymbol{K}, \boldsymbol{P}_K, \Sigma \rangle$ where $\boldsymbol{K}$ is a geometric shape (e.g., a triangle $\boldsymbol{S}\{\mathbf{q}_1, \mathbf{q}_2, \mathbf{q}_3\}$), $\boldsymbol{P}_K$ is a finite dimensional space of linear functions defined on $\boldsymbol{K}$ (e.g., $\boldsymbol{P}_1(\boldsymbol{S})$), and Σ is the *element degrees of freedom* (e.g., the values of some distribution at the vertices). A *triangular finite element space* is defined as the triple $\langle \Omega, \boldsymbol{T}_h(\Omega), \boldsymbol{V}_h(\Omega), \Sigma^G \rangle$ where $\boldsymbol{T}_h(\Omega)$ is a triangulation of Ω, $\boldsymbol{V}_h(\Omega)$ is the space of all continuous piece-wise linear functions defined on $\Omega \cap \partial\Omega$ whose restrictions to any element $\boldsymbol{S}$ of the triangulation is in $\boldsymbol{P}_1(\boldsymbol{S})$. More formally,

$$\begin{aligned} \boldsymbol{V}_h(\Omega) = \{(v \in C^0(\Omega \cap \partial\Omega)) | \\ (\forall(\boldsymbol{S} \in \boldsymbol{T}_h(\Omega)) \Rightarrow v|_{\boldsymbol{S}} \in \boldsymbol{P}_1(\boldsymbol{S}))\} \end{aligned} \quad (3)$$

Finally, Σ^G is the global degrees of freedom composed of all the values of $v \in \boldsymbol{V}_h(\Omega)$ at the vertices, i.e., $v(\mathbf{q}_1)$, $v(\mathbf{q}_2)$ and $v(\mathbf{q}_3)$ for every $\boldsymbol{S}\{\mathbf{q}_1, \mathbf{q}_2, \mathbf{q}_3\} \in \boldsymbol{T}_h(\Omega)$.

Consider, now, a field $\mathbf{f}: \Omega \to \Re$ and a formation $\boldsymbol{S}$ inside Ω. This formation plays the role of a single element. Define the rest of the tesselation using this reference element. Let $v \in \boldsymbol{P}_1(\boldsymbol{S})$. The degrees of freedom for $\boldsymbol{S}$ are $\mathbf{f}_{\boldsymbol{S}}$. We should have $v(\mathbf{q}_i) = \mathbf{f}(\mathbf{q}_i)$ which gives the linear system

$$\mathbf{f}_{\boldsymbol{S}} = \mathbf{1}_3 \mathbf{a}^T \begin{bmatrix} 1 & 1 & 1 \\ \mathbf{q}_1 & \mathbf{q}_2 & \mathbf{q}_3 \end{bmatrix}, \quad (4)$$

where $\mathbf{a} = [a_{00}, a_{10}, a_{01}]^T$. The linear interpolation of the field on this element is a mapping $\Psi^{\mathbf{I}}: \Re^{3\times 2} \times \Re^3 \to \Re^3$ which calculates the unique solution of the above system:

$$\mathbf{a}_{\boldsymbol{S}} = \Psi^{\mathbf{I}}(\mathbf{q}_{\boldsymbol{S}}, \mathbf{f}_{\boldsymbol{S}}) = \frac{1}{\Delta} \Theta \mathbf{f}_{\boldsymbol{S}} \quad (5)$$

where

$$\Theta = \begin{bmatrix} \begin{vmatrix} \mathbf{q}_2^T \\ \mathbf{q}_3^T \end{vmatrix} & \begin{vmatrix} \mathbf{q}_3^T \\ \mathbf{q}_1^T \end{vmatrix} & \begin{vmatrix} \mathbf{q}_1^T \\ \mathbf{q}_2^T \end{vmatrix} \\ (\mathbf{q}_2 - \mathbf{q}_3)^{\perp} & (\mathbf{q}_3 - \mathbf{q}_1)^{\perp} & (\mathbf{q}_1 - \mathbf{q}_2)^{\perp} \end{bmatrix}, \quad (6)$$

$$\Delta = \begin{vmatrix} \mathbf{q}_2^T \\ \mathbf{q}_3^T \end{vmatrix} + \begin{vmatrix} \mathbf{q}_3^T \\ \mathbf{q}_1^T \end{vmatrix} + \begin{vmatrix} \mathbf{q}_1^T \\ \mathbf{q}_2^T \end{vmatrix}. \quad (7)$$

We now define the *bilinear polynomial approximation* of $\mathbf{f}$ as the map $\tilde{\mathbf{f}}: \Omega \to \Re$ which is given by

$$\tilde{\mathbf{f}}(\mathbf{q}) = \mathbf{a}_{\boldsymbol{S}}^T \begin{bmatrix} 1 \\ \mathbf{q} \end{bmatrix}, \ \mathbf{q} \in \boldsymbol{S}. \quad (8)$$

Note that the model changes discontinuously from an element to its adjacent elements. The finer the triangulation (the smaller the formation sizes), the the better is $\tilde{\mathbf{f}}$ an approximation of $\mathbf{f}$. The contour lines of $\tilde{\mathbf{f}}$ (in any given element) are straight lines with slope $m_{\tilde{\mathbf{f}}} = -a_{10}/a_{01}$. Denoting $\theta_{\tilde{\mathbf{f}}} = \text{atan}(m_{\tilde{\mathbf{f}}})$, $v_{\tilde{\mathbf{f}}} = (\cos(\theta_{\tilde{\mathbf{f}}}), \sin(\theta_{\tilde{\mathbf{f}}}))^T$ gives the vector tangent to the lines and $\text{perp}(v_{\tilde{\mathbf{f}}})$ is the vector perpendicular (normal) to them, pointing in the direction of the minimum.

2.2 Isocline Representation

In the linear model, the contour approximating the isoline is given by $\mathbf{f}(\mathbf{q}) = \mathbf{c}_d$.

Define the mapping $\Psi_{\boldsymbol{I}}^{\boldsymbol{w}}: \Re^{3\times 2} \times \Re^3 \times \Re \to \Re^2 \times \Re^2$ which calculates the intersection of an isocline with a triangle. In other words, $(\boldsymbol{w}_1, \boldsymbol{w}_2) = \Psi_{\mathbf{I}}^{\boldsymbol{w}}(\mathbf{q}_{\boldsymbol{S}}, \mathbf{a}_{\boldsymbol{S}}, \mathbf{c}_d)$. For every edge $\{\mathbf{q}_i, \mathbf{q}_j\}$, we have

$$\boldsymbol{w}_{ij} = \frac{1}{\mu}((a_{00} - \mathbf{c}_d)(q_i - q_j) + \begin{bmatrix} a_{01} & a_{10} \end{bmatrix} \cdot \begin{bmatrix} |\boldsymbol{Q}_1| & |\boldsymbol{Q}_2| \end{bmatrix}), \quad (9)$$

where

$$\boldsymbol{Q}_1 = \begin{bmatrix} \mathbf{q}_i & \mathbf{q}_i \end{bmatrix}^T, \boldsymbol{Q}_2 = \begin{bmatrix} \mathbf{q}_j & \mathbf{q}_i \end{bmatrix}, \text{ and} \quad (10)$$

$$\mu = \begin{bmatrix} a_{10} & a_{01} \end{bmatrix} \cdot (\mathbf{q}_j - \mathbf{q}_i). \quad (11)$$

Only two of the three points $\boldsymbol{w}_{12}$, $\boldsymbol{w}_{13}$ and $\boldsymbol{w}_{23}$ correspond to intersections with the triangle. $\boldsymbol{w}_{ij}$ is an intersection if

$$\frac{|(\mathbf{q}_j - \mathbf{q}_i) \times (\mathbf{q}_i - \boldsymbol{w}_{ij})|}{\|\mathbf{q}_j - \mathbf{q}_i\|} = 0, \quad (12)$$

$$(\mathbf{q}_j - \mathbf{q}_i) \cdot (\boldsymbol{w}_{ij} - \mathbf{q}_i) \geq 0, \text{ and } \|\boldsymbol{w}_{ij} - \mathbf{q}_i\| \leq \|\mathbf{q}_j - \mathbf{q}_i\|. \quad (13)$$

The two points satisfying these are denoted as $\boldsymbol{w}_1$ and $\boldsymbol{w}_2$. Define $\Psi^{\boldsymbol{w}} = \Psi_{\mathbf{I}}^{\boldsymbol{w}} \circ \Psi^{\mathbf{I}}$. This interpolation is continuous across the common boundary between touching triangles ([Young and Gregory, 1988]).

If we redefine $\boldsymbol{w}_1$ and $\boldsymbol{w}_2$ as intersections of the isocline with a circle *circumscribed* around the triangle, $\Psi_{\mathbf{I}}^{\boldsymbol{w}}$ would have a closed form formula. Consider the line $\{\mathbf{q}^1, \mathbf{q}^2\}$ where $\mathbf{q}^1 = \bar{\mathbf{q}}_{\boldsymbol{S}} - l_{\varsigma} v_{\tilde{\mathbf{f}}}^{\perp}$, $\mathbf{q}^2 = \bar{\mathbf{q}}_{\boldsymbol{S}} + \varepsilon v_{\tilde{\mathbf{f}}}^{\perp}$, ε a positive constant. This line is normal to the model. Intersection of this line with the isoline gives

$$\mathbf{q}_Q = \frac{1}{\begin{bmatrix} a_{10} & a_{01} \end{bmatrix} \cdot (\mathbf{q}^2 - \mathbf{q}^1)} \Big((a_{00} - \mathbf{c}_d)(\mathbf{q}^1 - \mathbf{q}^2) + \begin{bmatrix} a_{01} & a_{10} \end{bmatrix} \cdot \begin{bmatrix} \begin{vmatrix} \begin{bmatrix} \mathbf{q}^{1T} & \mathbf{q}^{2T} \end{bmatrix}^T \end{vmatrix} & \begin{vmatrix} \begin{bmatrix} \mathbf{q}^2 & \mathbf{q}^1 \end{bmatrix} \end{vmatrix} \end{bmatrix} \Big) \quad (14)$$

Now, we compute the intersection of the line $\{\mathbf{q}_{\tilde{Q}}^1, \mathbf{q}_{\tilde{Q}}^2\}$, where $\mathbf{q}_{\tilde{Q}}^1 = \mathbf{q}_{\tilde{Q}} - \varepsilon v_{\tilde{F}}$ and $\mathbf{q}_{\tilde{Q}}^2 = \mathbf{q}_{\tilde{Q}} + \varepsilon v_{\tilde{F}}$, with the circle centred at $\bar{\mathbf{q}}_{\boldsymbol{S}}$ and with radius $L = L_d/(2\cos(\pi/6))$. Such a circle can be described by $\|\mathbf{q} - \bar{\mathbf{q}}_{\boldsymbol{S}}\| = L^2$. Substituting the equation of line $q = \mathbf{q}_{\tilde{Q}}^1 + u(\mathbf{q}_{\tilde{Q}}^2 - \mathbf{q}_{\tilde{Q}}^1)$ and solving the quadratic equation obtained gives the intersection points as

$$\boldsymbol{w}_i = \mathbf{q}_{\tilde{Q}}^1 + (\chi_1 + (3 - 2i)\chi_2)(\mathbf{q}_{\tilde{Q}}^2 - \mathbf{q}_{\tilde{Q}}^1), \quad (15)$$

$$\chi_1 = -\tilde{a}_{01}/2\tilde{a}_{00}, \quad (16)$$

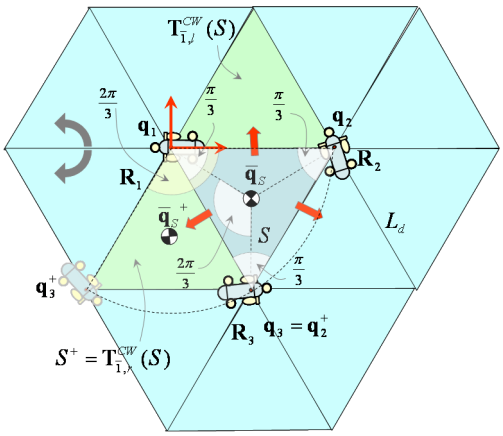

figure 3: The reflection operation $\boldsymbol{T}^{CW}_{\bar{1},r}$.

$$\chi_2 = \frac{1}{2\tilde{a}_{00}}(\tilde{a}_{01}{}^2 - 4\tilde{a}_{00}\tilde{a}_{10})^{1/2}, \tag{17}$$

$$\tilde{a}_{00} = \|\mathbf{q}_Q^2 - \mathbf{q}_Q^1\|^2, \tag{18}$$

$$\tilde{a}_{01} = 2(\mathbf{q}_Q^2 - \mathbf{q}_Q^1)^T(\mathbf{q}_Q^1 - \bar{\mathbf{q}}_S), \tag{19}$$

$$\tilde{a}_{10} = \|\bar{\mathbf{q}}_S\|^2 + \|\mathbf{q}_Q^1\|^2 - 2\bar{\mathbf{q}}_S{}^T\mathbf{q}_Q^1 - L^2. \tag{20}$$

If $\tilde{a}_{01}{}^2 - 4\tilde{a}_{00}\tilde{a}_{10} < 0$, no intersection occurs and if it is zero, $\boldsymbol{w}_1 = \boldsymbol{w}_2$.

3 Navigating the tesselation

Imagining that the formation is currently occupying an element of the tesselation, navigation means the ability to move to adjacent elements. This is possible by reflecting the triangle around one of the edges (figure 3). We denote the initial state of the triangle by $\boldsymbol{S}[0]$ and use $\boldsymbol{S}[k]$ to denote the current state. Having chosen an edge, $\boldsymbol{S}[k+1]$ can be produced by the matrix equation $\boldsymbol{T}\mathbf{q}_{\boldsymbol{S}[k]} = \mathbf{q}_{\boldsymbol{S}[k+1]}$ which basically assigns new values to vertices. Although $\boldsymbol{T}$ can be designed to effect true reflection (reversing the sense of the formation), we instead nominate one of the vertices as the *pivot* (which is to keep station) and move the other two to new positions (flip the triangle to left or right) such that $\boldsymbol{S}[k+1]$ would be equivalent to a reflected $\boldsymbol{S}[k]$. Let λ denote the desired direction of flipping: 1 for left and 0 otherwise. Let $\beta_i = 1$ if $\mathbf{q}_i$ is the pivot and 0 otherwise ($\beta_1 + \beta_2 + \beta_3 = 1$). For clock-wise formations, the general form of the transformation is

$$\boldsymbol{T} = \beta_1(\lambda\boldsymbol{T}_{\bar{1},l} + \bar{\lambda}\boldsymbol{T}_{\bar{1},r}) + \beta_2(\lambda\boldsymbol{T}_{\bar{2},l} + \bar{\lambda}\boldsymbol{T}_{\bar{2},r}) + \beta_3(\lambda\boldsymbol{T}_{\bar{3},l} + \bar{\lambda}\boldsymbol{T}_{\bar{3},r}) \tag{21}$$

where

$$\boldsymbol{T}_{\bar{1},r} = \begin{bmatrix}\boldsymbol{e}_1^T\\ \boldsymbol{e}_3^T\\ -\mathbf{1}_2^T\end{bmatrix}, \boldsymbol{T}_{\bar{1},l} = \begin{bmatrix}\boldsymbol{e}_1^T\\ -\mathbf{1}_3^T\\ \boldsymbol{e}_2^T\end{bmatrix}, \boldsymbol{T}_{\bar{3},l} = \begin{bmatrix}-\mathbf{1}_2^T\\ \boldsymbol{e}_1^T\\ \boldsymbol{e}_3^T\end{bmatrix}, \tag{22}$$

$$\boldsymbol{T}_{\bar{3},r} = \begin{bmatrix}\boldsymbol{e}_2^T\\ -\mathbf{1}_1^T\\ \boldsymbol{e}_3^T\end{bmatrix}, \boldsymbol{T}_{\bar{2},r} = \begin{bmatrix}-\mathbf{1}_3^T\\ \boldsymbol{e}_2^T\\ \boldsymbol{e}_1^T\end{bmatrix}, \boldsymbol{T}_{\bar{2},l} = \begin{bmatrix}\boldsymbol{e}_3^T\\ \boldsymbol{e}_2^T\\ -\mathbf{1}_1^T\end{bmatrix}$$

Here, $\boldsymbol{e}_1$, $\boldsymbol{e}_2$ and $\boldsymbol{e}_3$ denote the standard unit base vectors for $\Re^3$ and $-\mathbf{1}_i$ denotes a column vector with a -1 at position i and 1 in the other positions.

The task of a planning scheme is now to determine β_i and λ. Suitable control laws should then guide the moving robots to their destinations. In this paper, we use rotation around the pivot as control law.

Pick an anchor point $\mathbf{q}_w$ inside the triangle and fix an frame on it with arbitrary orientation. Denote by L_{wi} and ϑ_{wi}, $i = 1, 2, 3$, distances and bearings of robots with respect to this anchor. Given desired values L^d_{wi} and ϑ^d_{wi} for these, the formation can be maintained by using the control laws

$$\dot{\mathbf{q}}_i = \psi_i(L^d_{wi}, \vartheta^d_{wi}, \mathbf{q}_w, v_S(t), \omega_S(t)) + \kappa_1((R_z((\omega_{wi} + \omega_S(t))dt) - \mathbf{1}_2)(\mathbf{q}_i - \mathbf{q}_w)) + \kappa_2(L_{wi} - L^d_{wi})\frac{\mathbf{q}_i - \mathbf{q}_w}{\|\mathbf{q}_i - \mathbf{q}_w\|} + v_S(t) \tag{23}$$

$$\omega_{wi} = k(\vartheta_{wi} - \vartheta^d_{wi}). \tag{24}$$

$v_S(t)$ and $\omega_S(t)$ are linear and angualr velocities of the anchor, respectively. For rotation around the centre of mass, $\mathbf{q}_w = \bar{\mathbf{q}}_S$, and for rotation around the pivot, $\mathbf{q}_w = \mathbf{q}_p$. For this latter case, if the direction of flipping is left, the left neighbour of the pivot is called the *leader* $\mathbf{q}_l$ and the other one is called the *follower* $\mathbf{q}_f$. We have $L^d_{pp} = \vartheta^d_{pp} = 0$ and

$$\vartheta^d_{pf}[k] = \vartheta^d_{pf}[k-1] + \lambda(\pi/3), \tag{25}$$

$$\vartheta^d_{pl}[k] = \vartheta^d_{pf}[k-1] + \lambda(2\pi/3). \tag{26}$$

Also, $L^d_{pl} = L^d_{pf} = \boldsymbol{L}_d$ at all times. We will also use this general law, later on, for adjustment of the formation in relation to isoclines.

4 Planning

Traversing a domain can have two modes: moving along the gradient of the field and moving along the tangent to the gradient. See figure 4 for illustration.

4.1 Normal Motion

This operation follows the classical simplex method. It relies on classifying the vertices as *best*, *next-best* (or *next-worst*), and *worst*, such that $\mathbf{f}(\mathbf{q}_W) \le \mathbf{f}(\mathbf{q}_{NW}) \le \mathbf{f}(\mathbf{q}_B)$. Either of $\mathbf{q}_B$ or $\mathbf{q}_{NB}$ can be chosen as the pivot. By convention, we select the

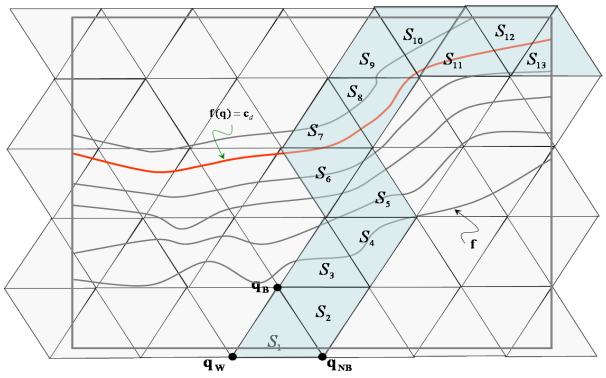

figure 4: Traversal of the tesselation.

vertex to the left of $\mathbf{q}_W$ as the pivot. Let ρ be 1 if the formation should go down hill, determined by the conditions $\mathbf{f}(\mathbf{q}_1) > \mathbf{c}_d$, $\mathbf{f}(\mathbf{q}_2) > \mathbf{c}_d$, $\mathbf{f}(\mathbf{q}_3) > \mathbf{c}_d$, and 0 if the conditions $\mathbf{f}(\mathbf{q}_1) < \mathbf{c}_d$, $\mathbf{f}(\mathbf{q}_2) < \mathbf{c}_d$ and $\mathbf{f}(\mathbf{q}_3) < \mathbf{c}_d$ are satisfied. Denote by $\mathbf{f}_{i,jk}$ the boolean variable which is true if $\mathbf{f}(\mathbf{q}_i) > \max\{\mathbf{f}(\mathbf{q}_j), \mathbf{f}(\mathbf{q}_k)\}$ and by $\tilde{\mathbf{f}}_{i,jk}$ the condition that $\mathbf{f}(\mathbf{q}_i) < \min\{\mathbf{f}(\mathbf{q}_j), \mathbf{f}(\mathbf{q}_k)\}$. Now, define

$$\beta_1 = (\rho \wedge \mathbf{f}_{3,12}) \vee (\bar{\rho} \wedge \tilde{\mathbf{f}}_{3,12}) \ , \tag{27}$$

$$\beta_2 = (\rho \wedge \mathbf{f}_{1,23}) \vee (\bar{\rho} \wedge \tilde{\mathbf{f}}_{1,23}) \ , \tag{28}$$

$$\beta_3 = (\rho \wedge \mathbf{f}_{2,13}) \vee (\bar{\rho} \wedge \tilde{\mathbf{f}}_{2,13}) \ . \tag{29}$$

For example, if $\beta_1 = 1$, we have $\boldsymbol{R}_l = \boldsymbol{R}_2$, $\boldsymbol{R}_f = \boldsymbol{R}_3$.

The formation will eventually reach the desired isocline when it intersects the interpolated isocline. In degenerate cases, where the isoline is touching a vertex or coincides an edge, we use the adjustment strategy described below.

4.2 Tangential Motion

Once the triangle has intersected the isocline, it can traverse it in either direction. Assume for now that the intersection is inside the triangle. Let us denote by $\boldsymbol{L}^w_{i,jk}$ the boolean variable which is true if $\{w_1, w_2\}$ intersects the edge $\{\mathbf{q}_j, \mathbf{q}_k\}$. We set

$$\beta_1 = \sigma_0(\boldsymbol{L}^w_{1,23} \wedge (\mathbf{f}_{1,23} \vee \tilde{\mathbf{f}}_{1,23})) \ , \tag{30}$$

$$\beta_2 = \sigma_0(\boldsymbol{L}^w_{2,13} \wedge (\mathbf{f}_{2,13} \vee \tilde{\mathbf{f}}_{2,13})) \ , \tag{31}$$

$$\beta_3 = \sigma_0(\boldsymbol{L}^w_{3,12} \wedge (\mathbf{f}_{3,12} \vee \tilde{\mathbf{f}}_{3,12})) \ , \tag{32}$$

where $\sigma_0(u)$ is 1 if u is true, and 0 otherwise. The direction of flipping is determined by the formula

$$\lambda = \tilde{d}\sigma_{-1}(\mathbf{f}_{p,lf}, \tilde{\mathbf{f}}_{p,lf}) \ , \tag{33}$$

where $\sigma_{-1}(u_1, u_2)$ is -1 if u_1 is true, and 1 if u_2 is true. It is undefined if both u_1 and u_2 are false. $\tilde{d}$ is a user-defined direction of traversal. It should be 1 for left and -1 for right.

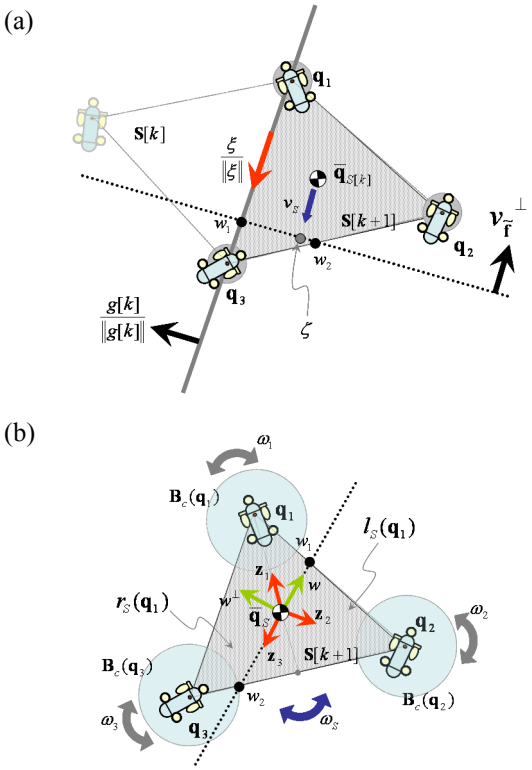

figure 5: Location adjustment with (a) translation and (b) rotation.

Let $\gamma_d : \Re \to \Re^2$ denote the closed curve (isoline) of the field $\mathbf{f}$, induced by the desired field value $\boldsymbol{c}_d$, and parametrized by $\boldsymbol{s} \in \Re$. Moving in a certain direction will always see $\boldsymbol{s}$ either increasing or decreasing. Let $\grave{\boldsymbol{N}}_{\gamma_d}(\boldsymbol{s})$ be the inward normal to the curve at $\boldsymbol{s}$. Under the above rules, the formation will always traverse the isoline in the same direction if at each $\boldsymbol{s}$, all the vectors $\nu\grave{\boldsymbol{N}}_{\gamma_d}(\boldsymbol{s})$, $\nu \in [-1, 1]$, have positive (semi-definite) slope.

4.3 Location Adjustment

As contact between the interpolated isocline and the triangle approaches the vertices or sides, uncertainty regarding reflection increases. To address this, we associate circular *critical regions* $\boldsymbol{B}_c(\mathbf{q}_i)$ (with a radius δ_c) with vertices (figure 5). It is preferable that $L\{w_1, w_2\}$ lie in the *safe region*, as close to passing through $\bar{\mathbf{q}}_S$ as possible. This will also make line segments more equal. To do this, after each reflection, we translate and rotate the formation appropriately. To translate and rotate the formation, we use the control law given in (23), setting $\mathbf{q}_w = \bar{\mathbf{q}}_S$,

$$L^d_{\bar{\mathbf{q}}_S,1} = L_{\bar{\mathbf{q}}_S,2} = L_{\bar{\mathbf{q}}_S,3} = \frac{L_d}{2\cos(\pi/6)} \ , \tag{34}$$

$$\vartheta^d_{\bar{\mathbf{q}}_S,1} = \vartheta_{\bar{\mathbf{q}}_S,1} \ , \ \vartheta^d_{\bar{\mathbf{q}}_S,j} = \vartheta^d_{\bar{\mathbf{q}}_S,1} + (j-1)\frac{2\pi}{3} \ , \tag{35}$$

where $j = 2, 3$.

One strategy for translation is to slide the formation along $\xi[k] = \mathbf{q}_i[k] - \mathbf{q}_p[k]$, k being the index of the last generated simplex. Thus,

$$v_{\boldsymbol{S}} = \mu_1 k \langle \zeta - \bar{\mathbf{q}}_{\boldsymbol{S}}, \xi \rangle \frac{\xi}{\|\xi\|} + (1 - \mu_1) k (\zeta - \bar{\mathbf{q}}_{\boldsymbol{S}}), \quad (36)$$

where ζ is the closest point on $L\{w_1, w_2\}$ to $\bar{\mathbf{q}}_{\boldsymbol{S}}$. μ_1 is 1 if ξ is defined and 0 otherwise. Translation stops when $\{w_1, w_2\}$ falls inside the safe region. Note that, if the current $L\{w_1, w_2\}$ is nearly perpendicular to the sliding constraint, the goal may not be achieved. This situation signals that the triangle is too big. An alternative control is to let the formation move freely in the *half-plane* that does not overlap with the last generated triangle. The constraint is then defined as

$$\langle \zeta - \bar{\mathbf{q}}_{\boldsymbol{S}}, \frac{\boldsymbol{g}[k]}{\|\boldsymbol{g}[k]\|} \rangle \leq 0, \; \boldsymbol{g}[k] = \bar{\mathbf{q}}_{\boldsymbol{S}[k]} - \varsigma[k], \quad (37)$$

$\varsigma[k]$ being the closest point on the line defined by $\xi[k]$ to $\mathbf{q}_{\boldsymbol{S}[k]}$. This may fragment the sequence of segments, though. Note that, as $\|w_2 - w_1\|$ gets smaller, the computations become ill-defined. So, instead of calculating closest points, we can use the rule

$$v_{\boldsymbol{S}} = -(\mathbf{c}_d - \tilde{\mathbf{f}}(\bar{\mathbf{q}}_{\boldsymbol{S}})) \mathrm{perp}(v_{\tilde{\mathbf{f}}}). \quad (38)$$

As for rotation, we can imagine critical regions as repelling areas and define $\omega_{\boldsymbol{S}} = \omega_1 + \omega_2 + \omega_3$, where ω_i is the contribution of $\boldsymbol{R}_i$. We set $\omega_i = 0$ if $w_1, w_2 \notin \boldsymbol{R}_c(\mathbf{q}_i)$ or $w_1, w_2 \in \boldsymbol{R}_u(\mathbf{q}_i)$ or one of w_1 or w_2 is in $\boldsymbol{R}_u(\mathbf{q}_i)$ and the other is in $\boldsymbol{R}_u(\mathbf{q}_j)$ or $\boldsymbol{R}_c(\mathbf{q}_j)$ for some $j \neq i$. Otherwise, we set $\omega_i = \varpi$ if one of w_1 or w_2 is in $\boldsymbol{R}_u(\mathbf{q}_i)$ and the other is in the right half of the triangle $r_{\boldsymbol{S}}(\mathbf{q}_i)$ (viewed from $\boldsymbol{R}_i$'s position), and $\omega_i = -\varpi$ if it is in the left half $l_{\boldsymbol{S}}(\mathbf{q}_i)$. Here, ϖ is a nominal angular speed. If neither of the above applies, both w_1 and w_2 are in $\boldsymbol{R}_c(\mathbf{q}_i)$ and we set

$$\omega_i = \sum_{j=1,2} \chi_j(w_j) \eta(w_j, \boldsymbol{R}_c(\mathbf{q}_i)) U_c(\|\mathbf{q}_i - w_j\|), \quad (39)$$

where $U_c(u)$ is a monotonically decreasing function, going to zero at the boundary of a critical region, $\eta(w, \boldsymbol{B})$ is 1 if $w \in \boldsymbol{B}$ and 0 otherwise, $\chi_i(w)$ is -1 if w lies on the link between $\mathbf{q}_i$ and its right neighbour and 1 if this applies to the left neighbour. An example choice for $U_c(u)$ is $k \exp(u^2/\sigma_c^2)$ where $\sigma_c \leq \delta_c / \sqrt{-\ln(\varepsilon)}$ (to make sure that $U_c(u) \leq \varepsilon$ at the boundary of $\boldsymbol{R}_c(\mathbf{q}_i)$). It is to see that these rules are not in conflict and the outcome is a unique angular velocity. It may be the case that the contributions of two vertices balance each other in which case adjustment will only involve translation.

Another simpler strategy for rotation is to find the $\boldsymbol{z}_i$ which has the least angle with either $w^{\perp}$ or $-w^{\perp}$, where $w = \mathbf{n}(w_2 - w_1)$, and rotate the formation to align $\boldsymbol{z}_i$ with it. This works because if any of the vectors $\boldsymbol{z}_i$ is perpendicular to the model, the isoline would be in the safe region. Note that we are assuming that the triangular is almost regular. See figure 5(b).

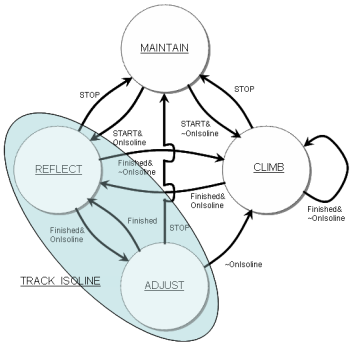

figure 6: Operation state diagram.

4.4 System Overview

Figure 6 shows the hybrid state diagram of the whole operation cycle. This automaton is synchronously executed by the agents. We might think of a designated leader with the other two as followers or implement the automaton in each robot and provide synchronization points. We will not discuss these issues any further here.

5 Simulations

Figure 7(a) shows reaching and tracking an isoline without location adjustment. As can be seen, the generated triangles are adacent elements of the tesselation. Note the irregularly sized segments of the approximation. In contrast, figure 7(b) shows a formation employing location adjustment (also shown is the trace of the centre of mass). The line segments tend to be more equal and uncertainty in determining the flipping direction is reduced. On the other hand, there are gaps in the approximation and the generated triangles do not correspond to a unified tesellation. Figure 8 shows formations of different sizes against the same environment. Note the anomalous situation in figure 8(a) where S_4, while tracking the isoline, settles down in a position which is almost coincident with S_2 but with a 180 degree rotation. In figure 8(b), S_8 travels a long way before ending up in S_9 at which point it is no longer on the isoline. S_{12}, S_{13} and S_{14} are also not on the isoline (although they are on the physical isoline, they have failed to register it). Due to numerical errors in the simulation, S_{14} is slightly different from S_{12} which enables the formation to finally get back on the line. In figure 8(c), the formation again travels long distances before stabilizing on the line, producing a fragmented approximation. This seemingly discouraging performance degradation (as compared to the unadjusted case) should not be regarded as inappropriateness of adjusting. All the cases shown correspond to situations where formation size is too big against the curvature of the

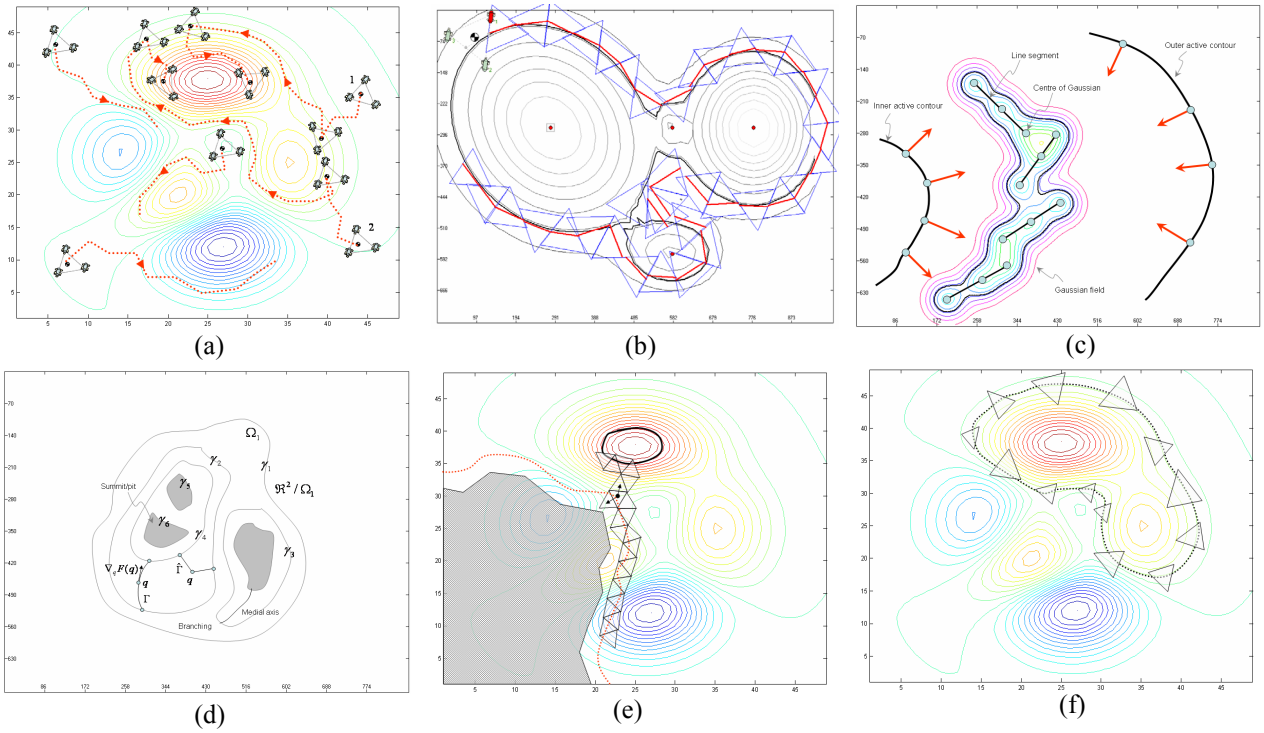

figure 9: Ingredients of a complete system. (a) Multiple formations. (b) Line segment approximation. (c) Landscape generation and active contours. (d) Terrain interpolation. (e) Avoiding areas. (f) Size-adjustment.

isoline and, accordingly, gives us a clue as to the importance of size adaptation (see next section).

6 Other Considerations

In this section, we will consider a number of issues which have to be addressed in a complete framework.

6.1 Cooperative Formations

Here, we only addressed a tiny part of the scenario described in the introduction. Self-organization of formations from a aggregate is not trivial and involves significant amounts of communication and synchronization among robots. Deciding on which isoclines to sample has not been satisfactorily addressed. It seems reasonable that isoclines in areas with high gradients are more significant (carry more information). Dispersal and rendezvous requires capabilities such as GPS. Strategies for collision avoidance and safe navigation in close proximity to peer formations is also a basic component. Figure 9(a) shows different formations independently and simultaneously sampling different isoclines. Also shown are two formations sampling a single isocline.

6.2 Terrain Reconstruction

Considering a single isocline, the outcome of the mission is a set of line segments (figure 9(b)). To create smooth curves, we propose to define Gaussians (with user-defined peak value and variance) on equally-distanced points on each segment and sum them up to produce a landscape (figure 9(c)). We then consider a certain level set of this landscape. Active contours [Kass et al., 1988]can now be initialized inside and outside the set of segments and let to evolve and adapt to the inner and outer edges of the level set (figure 9(c)). The average of the final states can be used as a representation of the isoline. Parameters of the contours determine smoothness of the final result. Given a set of smooth isoclines, the methods proposed in [Horman et al., 2003] can be used to reconstruct the terrain (figure 9(d)). Given a point $\mathbf{q}$ between two isoclines γ_1 and γ_2 with field values h_1 and h_2, we can use *univariate interpolation* along the *gradient path* Γ (shortest path along the terrain from $\mathbf{q}$ to the isolines). Supposing that $\Gamma = (\mathbf{q}_1, \mathbf{q}, \mathbf{q}_2)$ is the first approximation of Γ ($\mathbf{q}_1$ and $\mathbf{q}_2$ being the closest points on γ_1 and γ_2 to $\mathbf{q}$), linear interpolation gives

$$\mathbf{f}(\mathbf{q}) = \frac{h_2\|\mathbf{q}-\mathbf{q}_1\| + h_1\|\mathbf{q}-\mathbf{q}_2\|}{\|\mathbf{q}-\mathbf{q}_1\| + \|\mathbf{q}-\mathbf{q}_2\|}. \qquad (40)$$

Such an $\mathbf{f}$ is C^1-continuous except at the medial axis of γ_i and the boundary of Ω_i and $\Re^2\backslash\Omega_i$ where it is C^0-continuous. Refer to [Horman et al., 2003] for details and improved schemes (such as *Hermite* interpolation).

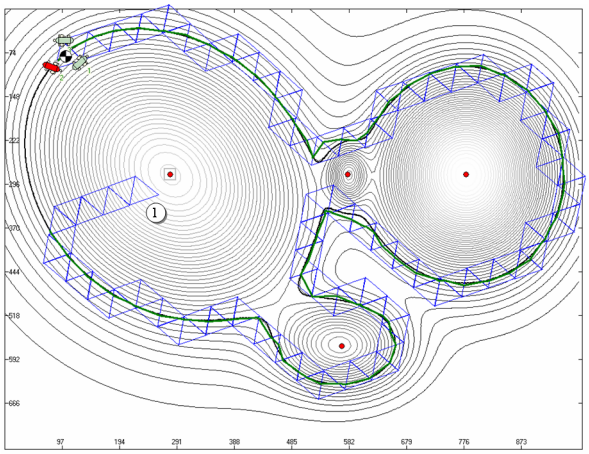

(a)

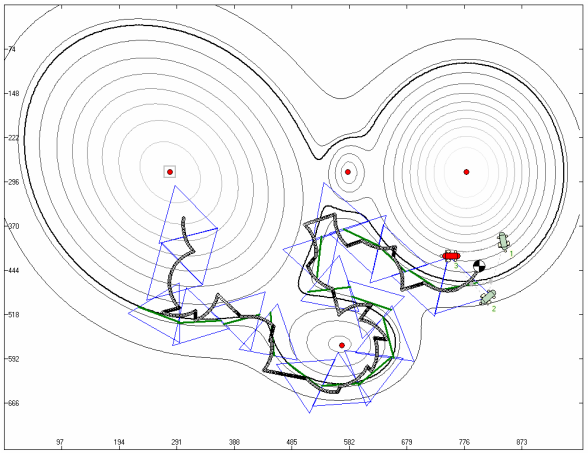

(b)

figure 7: Isocline tracking (a) with and (b) without adjustment.

6.3 Obstacle Avoidance

Avoiding obstacles can be approached simply by defining a potential field U_O around the boundary of the obstacle. Qualitatively, $U_O(\mathbf{q}) \to 1$ as $D(\mathbf{q}, \gamma_O) = \|\mathbf{q} - Q(\mathbf{q}, \gamma_O)\| \to 0$, and $U_O(\mathbf{q}) \to 0$ as $D(\mathbf{q}, \gamma_O) \to \infty$. Now, avoidance behaviour consists of traversing an isocline of the potential given by $U_O(\mathbf{q}) = u_0$. Assume that the distance between this isoline and the terrain isoline is sufficiently big. The formation switches to obstacle avoidance when there is a conflict between the action required for climbing and that for obstacle potential isoline traversal. Similarly, normal climbing is resumed as soon as no conflict exists. See figure 9(e).

6.4 Size Adjustment

Simulations clearly indicate the need for an adaptive strategy in which the size of the formation changes (figure 9(f)) to account for change in local curvature of the isocline. This also

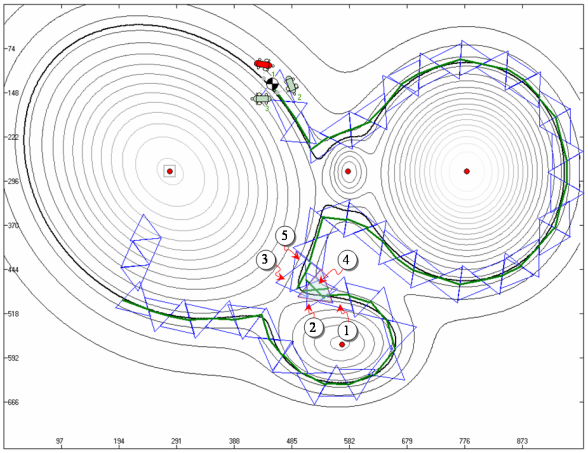

(a)

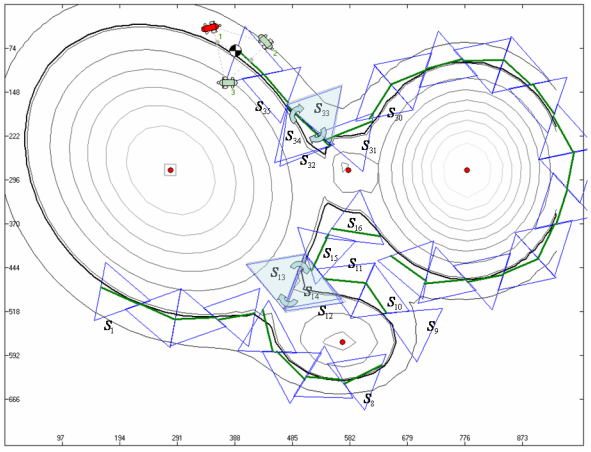

(b)

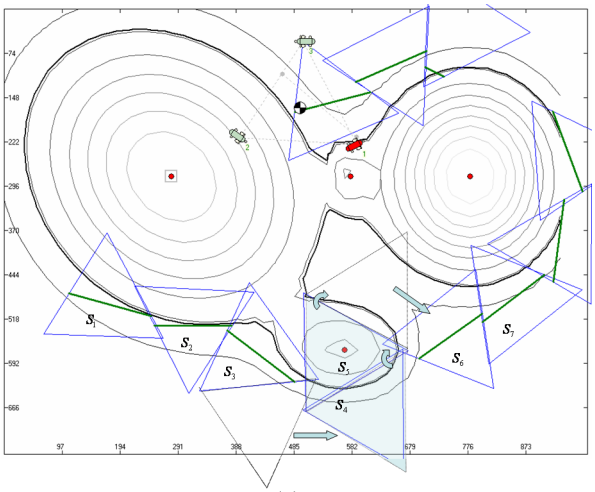

(c)

figure 8: Formations of different sizes. (a) $L_d = 50$. (b) $L_d = 100$. (c) $L_d = 200$.

has direct relation to decreasing the interpolation error. The general equation governing such a strategy is

$$\dot{\boldsymbol{A}}_S = f(\boldsymbol{A}_S, \boldsymbol{E}_e, \boldsymbol{A}_n)\,. \tag{41}$$

where $\boldsymbol{A}_n$ is some predefined nominal desired size, and $\boldsymbol{E}_e$ is some measure of suitability of the current size for the local situation. $\boldsymbol{E}_e$ can, of course, be a function of a direct estimate of the curvature which does not seem practical. We may instead use an indirect measure and a threshold against which suitability can be compared. We will defer discussion of this topic to future publications.

6.5 Noise

We only considered the noise-free case in which the field is static and smooth, and the sensors measure the true value of the field at each location. In reality, this is far from being true. As far as the field itself is concerned, we can model it as a smooth underlying function corrupted with some noise. Slowly varying fields can be modeled by a non-static white noise. White noise is also traditionally used to model more realistic sensors. Since actuation is not perfect, vehicles are in constant motion even when they are trying to keep station by counteracting the ambient flow. For this reason, when we talk about a sensor value, we are actually refering to some average of the values read by the sensor in a certain time frame in a neighbourhood of the location occupied by the vehicle. This average is, of course, changing but once the vehicles synchronize, the momentary value is used to decide on the next action. Note that the accumulated uncertainty (due to both field and sensor noise) can be quite large indeed without affecting the direction of reflection. This is the main property that makes this strategy so appealing. We refer the reader to future publications for more detailed analysis and demonstrations.

7 Conclusions

In this paper, we examined a strategy for surveying an underwater phenomenon. We proposed the use of the simplex nonlinear optimization algorithm for localizing optima of function defined on the plane. In this method, three autonomous vehicles are arranged in a triangular formation. Instead of continuous motion of a designated point inside the formation (such as the centre of mass), in each iteration, two of the robots rotate around the third designated leader. This behaviour effectively implements relection which is the only operation defined by the simplex algorithm. The most important features of this strategy are (1) ease of implementation, (2) robustness to noise in measurements, (3) robustness against non-smooth environments, (4) use of the field itself as a beacon for localization, and (5) adaptive sampling of important area.

We extended the basic algorithm (which obly considers climbing the gradient direction) to incorporate moving along iso-contours. We also discussed a general framework. Future publications will deal with uncertainty and implementation issues in more detail.

References

[Serafina web site]
http://users.rsise.anu.edu.au/~serafina/

[Rendas *et al.*, 2002]
Rendas, M.J., Folcher, J.-P., Lourtie, I.M., *Contour Tracking with Video and Altmeter, Project SUMARE Deliverable 4.1 (*http://www.mumm.ac.be/SUMARE/*),* 2002.

[Reet, 2005]
Reet, A.V., *Contour Tracking for the REMUS Autonomous Underwater Vehicle, Master's thesis, Dept. of Mech. Eng., US Naval Postgraduate School,* 2005.

[Zhang and Leonard, 2005]
Zhang, F., Leonard, N.E., *Generating Contour Plots using Multiple Sensor Platforms, Proc. IEEE Swarm Intelligence Symp.,* 2005.

[Ogren *et al.*, 2002]
Ogren, P., Fiorelli, E., Leonard, N.E., *Formations with a Mission: Stable Coordination of Vehicle Group Maneuvres, Proc. 15th Int. Symp. on Math. Theory of Networks and Systems,* 2002.

[Horman *et al.*, 2003]
Hormann, K., Spinello, S., Schroder, P., *C^1-Continuous Terrain Reconstruction from Sparse Contours, 8th Int. Fall Workshop on Vision and Visualization, Munich, Germany,* 2003.

[Robinet, 2004]
Robinet, III, R.D., *Stability and Control of Collective Systems, Journal of Intelligent and Robotic Systems, Vol. 39,* 2004.

[Pang *et al.*, 2003]
Pang, S., Farrell, J.A., Arrieta, R.M., Li, W., *AUV Reactive Planning: Deepest Point, Proc. of IEEE Oceans Conf., San Diego, USA,* 2003.

[Burian *et al.*, 1996]
Burian, E., Yoerger, D., Bradley, A., Singh, H., *Gradient Search with Autonomous Underwater Vehicles Using Scalar Measurements, Proc. of IEEE Symp. on Autonomous Underwater Vehicle Technology, Monterey, CA, USA,* 1996.

[Kolda *et al.*, 2003]
Kolda, T.G., Lewis, R.M., Torczon, V., *Optimization by Direct Search: New Perspectives on Some Classical and Modern Methods, SIAM Review, 45(3),* 2003.

[Kalantar and Zimmer, 2007]
Kalantar, S., Zimmer, U., *Simplex Formations of Autonomous Vehicles and Adaptive Sampling Strategies, Submitted to TAROS'07, Aberystwyth,* Sept. 2007.

[de Sousa *et al.*, 2005]
de Sousa, J.B., Johansson, K.H., Speranzon, A., Silva, J., *A Control Architecture for Multiple Submarines in Coordi-*

nated Search Missions, Proc. of the 16th IFAC World Congress, 2005.

[Speranzon *et al.*, 2004]
Speranzon, A., Silva, J., de Sousa, J.B., Johansson, K.H., *On Collaborative Optimization and Communication for a Team of Autonomous Underwater Vehicles, Proc. of Regelmote,* 2004.

[Young and Gregory, 1988]
Young, D.M., Gregory, R.T., *A Survey of Numerical Mathematics, Dover, New York,* 1988.

[Kass et al., 1988]
Kass, M., Witkins, A., Terzopoulos, D., *Snakes: active contour models, Int. Journal Computer Vision, 1(4):321-- 331,* 1988.